AGU PUBLICATIONS

Radio Science

RESEARCH ARTICLE

10.1002/2016RS005967

Key Points:

- Observations of conjugate nighttime MSTIDs (electrobuoyancy waves) during magnetically disturbed periods
- GPS TEC signatures of MSTIDs in two opposite hemispheres under different interhemisphere background conditions
- Evidence of interhemispheric coupling of MSTIDs in the American Sector

Supporting Information:

- Supporting Information S1
- Movie S1

Correspondence to:
C. E. Valladares,
cesar.valladares@bc.edu

Citation:
Valladares, C. E., and R. Sheehan (2016), Observations of conjugate MSTIDs using networks of GPS receivers in the American sector, *Radio Sci.*, *51*, 1470–1488, doi:10.1002/2016RS005967.

Received 2 FEB 2016
Accepted 6 AUG 2016
Accepted article online 10 AUG 2016
Published online 16 SEP 2016

Observations of conjugate MSTIDs using networks of GPS receivers in the American sector

C. E. Valladares[1,2] and R. Sheehan[1]

[1]Institute for Scientific Research, Boston College, Newton, Massachusetts, USA, [2]Hanson Center for Space Sciences, University of Texas at Dallas, Richardson, Texas, USA

Abstract This study has used total electron content (TEC) values from an extended network of GPS receivers and a highly developed processing to characterize the conjugacy of medium-scale traveling ionospheric disturbances (MSTIDs) over the American continent. It was found that midlatitude nighttime MSTIDs, also named electrobuoyancy waves, map into the opposite hemisphere but the amplitude of the TEC disturbance in the Southern Hemisphere is between 8 and 13% of the amplitude in the original hemisphere. The periods of the MSTIDs vary between 50 and 65 min. MSTID dynamics is presented for two days: 20 August 2012 and 17 June 2012. On the first day, MSTIDs entered into the American sector shortly before 4 UT, last for 3 h, drifted at an average speed of 200 m/s, and dissipated in the Caribbean region. In the Northern Hemisphere, the MSTIDs were directed southwestward (SW) and 60° from south. In the Southern Hemisphere, they moved northwestward (NW) or ~60° from north. The MSTID velocity changed through the night from ~300 m/s to ~150 m/s, but the propagation direction did not vary. On 17 June 2012 a series of wide MSTIDs were seen traveling across the Caribbean region that exited through the western coast of Central America. These MSTIDs last for ~5 h. Number density measured with the DMSP-F15 and DMSP-F17 satellites confirm the notion that the MSTIDs consist of rising and falling sheets of plasma density driven by electric fields likely set by a Perkins-type instability. These observations support the notion that gravity waves can seed and boost the growth of the nighttime MSTIDs.

1. Introduction

Nighttime medium-scale traveling ionospheric disturbances (MSTIDs) are buoyancy waves that have been electrified following a Perkins-type instability [*Perkins*, 1973]. MSTIDs occur at midlatitude regions where the magnetic field lines are tilted. One of the first measurements to study the morphology of MSTIDs was conducted with the Arecibo incoherent scatter radar (ISR) which observed the presence of well-defined bands of enhanced density, associated with large electric fields and elongated in the northwest-southeast (NW-SE) direction [*Behnke*, 1979]. Additional ISR measurements revealed that the large electric fields could originate at the opposite hemisphere and map along the magnetic field lines [*Burnside et al.*, 1983]. Later, the Middle and Upper atmosphere (MU) coherent radar in Japan showed a correspondence between these events and the more violent midlatitude spread *F* [*Fukao et al.*, 1991]. These experiments led *Kelley and Fukao* [1991] to suggest that gravity waves (GW) may be producing required density structures which are then amplified by the Perkins instability. Airglow imagers placed in opposite hemispheres at conjugate locations corroborated the MSTIDs mapping properties and their motion in the SW direction [*Saito et al.*, 2002; *Otsuka et al.*, 2004; *Shiokawa et al.*, 2005; *Martinis et al.*, 2011]. Networks of GPS receivers were used to show that the nighttime MSTIDs extend for distances longer than 2000 km in the NW-SE direction, occupying latitudes between 35 and 55°N magnetic latitude (MLAT) [*Tsugawa et al.*, 2007].

Satellites later observed rising and falling sheets of plasma consistent with theoretical predictions of the Perkins instability [*Hanson and Johnson*, 1992]. Further studies using DE 2 satellite data showed the presence of electric field fluctuations in both hemispheres [*Saito et al.*, 1995]. Measurements of polarization electric fields conducted with the DMSP-F15 satellite revealed the excellent spatial correlation between the field variability and the MSTID structure in the airglow image [*Shiokawa et al.*, 2003]. Almost at the same time, satellite-based observations indicated the presence of blobs (regions of enhanced plasma in the topside ionosphere) [*Park et al.*, 2003, 2008]. It was later realized that the blob morphology was different and could not be associated with equatorial plasma depletions [*Choi et al.*, 2012]. Joint ground and satellite-based observations indicated that the 630.0 nm airglow bands were anticorrelated with density blobs measured

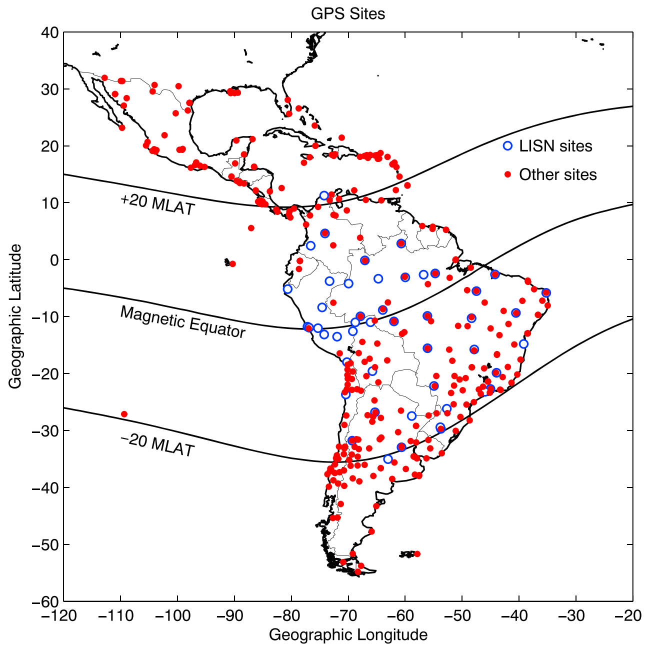

Figure 1. Locations of GPS receiver stations installed by the LISN project (blue) and several other networks (red) in South and Central America and the Caribbean region.

by the C/NOFS satellite. This relationship was explained in terms of the modulation of the density profiles due to electric fields created within the MSTID [*Miller et al.*, 2014].

All these studies have concluded that nighttime MSTIDs consist of several bands of high and low 630.0 nm airglow intensity [*Mendillo et al.*, 1997]. They generally move westward and equatorward at phase velocities of 50–150 m/s [*Garcia et al.*, 2000]. They are magnetically conjugate and preferentially occur during the solstices [*Martinis et al.*, 2010; *Makela et al.*, 2010; *Duly et al.*, 2013].

To explain the preferred southwestward propagation direction, *Kelley and Makela* [2001] invoked a mechanism in which a polarization electric field was directed parallel to the density-enhanced bands. Although the NW-SE alignment of the MSTIDs was in agreement with the Perkins instability, it was difficult for their theoretical model to explain the fast growth rate that was observed. Previously, *Kelley and Miller* [1997] and *Miller et al.* [1997] had argued that gravity waves could excite electric fields that are unstable. This hypothesis is still a viable explanation for the generation of MSTIDs. Recently, *Fukushima et al.* [2012] have concluded, based on an analysis of 7 years of airglow images from Kototabang in Indonesia, that MSTIDs were caused by GWs within the thermosphere.

Recently, high emphasis has been dedicated to understand the magnetic conjugate characteristics of the MSTIDs and the coupling to instabilities in sporadic E_s layers. These studies have shown that electric fields mapping to the opposite hemisphere can generate conjugate MSTIDs that mirror the disturbance of the originating hemisphere [*Yokoyama et al.*, 2009; *Martinis et al.*, 2010, 2011; *Yokoyama and Hysell*, 2010].

E and *F* region coupling can be very important for the stability of the nighttime midlatitude ionosphere [*Tsunoda and Cosgrove*, 2001]. Feedback and coupling, and in particular polarization processes in the *E* region, can lead to positive feedback and enhanced growth rates [*Cosgrove*, 2002, 2004]. The numerical simulation results of *Yokoyama et al.* [2009] showed that E_s layer instability plays a major role in seeding the structure of electron density in the *F* region.

In this paper, GPS total electron content (TEC) values and TEC perturbations take center stage to describe the characteristics, the mapping properties, and the conjugacy of MSTIDs observed on two days in 2012 (section 2). A description of the MSTID velocity calculations and the results (for both hemispheres) are presented in section 3. The observations are complemented with in situ number density collected by the DMSP-F15 satellite (section 4). The paper continues with a discussion (section 5) and a conclusion section (section 6).

2. Ground-Based Observations

The Low-Latitude Ionospheric Sensor Network (LISN) is a distributed observatory designed to specify the condition of the ionosphere over South America in a regional context. The LISN observatory employs real-time downloads to provide a nowcast of the South American ionosphere based upon observables from 45 dual-frequency GPS receivers [*Valladares and Chau*, 2012], 5 magnetometers placed along two different base lines, and 4 Volumetric Imaging and Processing of Integrated Radar (VIPIR) ionosondes. Figure 1 shows the locations of the LISN GPS receivers (blue open circles) and several other networks of GPS receivers (red full circles) that operate in South and Central America and the Caribbean region. A total of 382 permanent GPS receivers operated in South and Central America in 2012. As part of the LISN effort, the RINEX (Receiver Independent Exchange Format) files from all of the GPS receivers of Figure 1 are processed and stored in the LISN server for display and dissemination. In addition, a variety of plots including hourly maps of TEC values, occurrence of TIDs, and TEC depletions over South and Central America are constructed and available in the LISN website. Figure 1 also displays the locations of the magnetic equator and the ±20° magnetic latitude lines across the continent. By using TEC values from receivers located in Central America and the Caribbean regions, it is possible to study midlatitude MSTIDs that develop between 115° and 55° W longitude. Simultaneously, the effect of the MSTID mapping to the opposite hemisphere can be also observed with the GPS that exists in Southern Argentina and Chile (between 75° and 55° W longitude).

Figure 2 presents a summary of the MSTID activity in the American sector observed in the Northern Hemisphere at magnetic latitudes between 24° and 40° (top) and in the Southern Hemisphere at magnetic latitudes south of −24° (bottom). This figure was obtained by using an analysis software that automatically detects TEC depletions and structures [*Seemala and Valladares*, 2011]. This method consists of calculating the TEC daily variability by individually fitting a fourth-order polynomial to the TEC trace for each GPS satellite pass and for each station in South and Central America. The fitted TEC curves are then subtracted from the corresponding measured TEC. When the TEC difference is below a certain threshold that is commonly set to −1 TECU (total electron content unit, 1 TECU = 10^{16} el m^{-2}), a possible TEC depletion is marked. A second TEC fitting is conducted for each TEC trace excluding the times when TEC depletions were detected in the first pass. This second step guarantees a better determination of the unperturbed daily variability. The final step searches for the starting and ending times of the depletions by examining small changes in the time derivative of the TEC curves. This analysis code was applied to the TEC values derived from each GPS satellite pass, for each station of Figure 1 and for each day of 2012. Figure 2 indicates that occasionally, TEC depletions persist up to daytime hours, but they only occur during days of high magnetic activity. *Kp* values are printed in Figure 2 to point out this close relationship between morningside TEC depletions and high magnetic activity. We believe that these morning/afternoon TEC depletions are associated with equatorial plasma bubbles that rise to high altitudes driven by a prompt penetrating electric field or a disturbance dynamo [*Ma and Maruyama*, 2006; *Li et al*., 2012]. A careful analysis of these events is beyond the scope of this paper and will not be dealt with here. It is worthy to note that in 2012, there existed other days that were highly disturbed, but no morning/early afternoon structures were found in the American sector.

The main point of Figure 2 is to point out that during non–highly disturbed conditions MSTIDs occur between the months of April and August. In contrast the TEC structures in the Southern Hemisphere with amplitudes larger than 1 TECU are only observed during the December solstice. It is indicated that initially, our processing software was restricted to detect depletions with depths larger than 1 TECU. For this reason, our initial attempts to find conjugate MSTIDs in the Southern Hemisphere failed. The conjugate MSTIDs in the Southern Hemisphere were smaller than the 1 TECU threshold. Figure 2 was constructed using the 1 TECU threshold for both hemispheres. The following figures describe the characteristics and the conjugate properties of a few MSTID events that developed in the American sector during quiet and moderately disturbed magnetic conditions.

2.1. MSTIDs Observed on 20 August 2012

On 20 August 2012 the magnetic activity was moderately active during which the *Kp* index varied between 3 + and 3^0 during the first two 3 h periods. On this day a series of MSTIDs drifted into the eastern side of the field of view (FOV) of the GPS network that operates in the Caribbean region. The TEC perturbations (TECP) of Figure 3 were derived using signals from the GPS satellite 15. These 25 stations are located in the Caribbean region and in the northern part of South America (see red dots in Figure 3, right). These TECP values were derived by removing the daily TEC variability using a polynomial fit to every 3 h of data [*Valladares and Hei*, 2012]. MSTIDs were observed starting shortly before 04 UT and persisted until 0730 UT. On this day, significant TECP developed in Central America and the Caribbean region, but no plasma depletions/structures were observed in South America except for small-amplitude conjugate MSTIDs seen in the southern part of Argentina and Chile. Figure 3 (left) also displays the name of the city and the geographic locations of all 25 stations. The stations are arranged from geographic north to south to illustrate the general motion of the

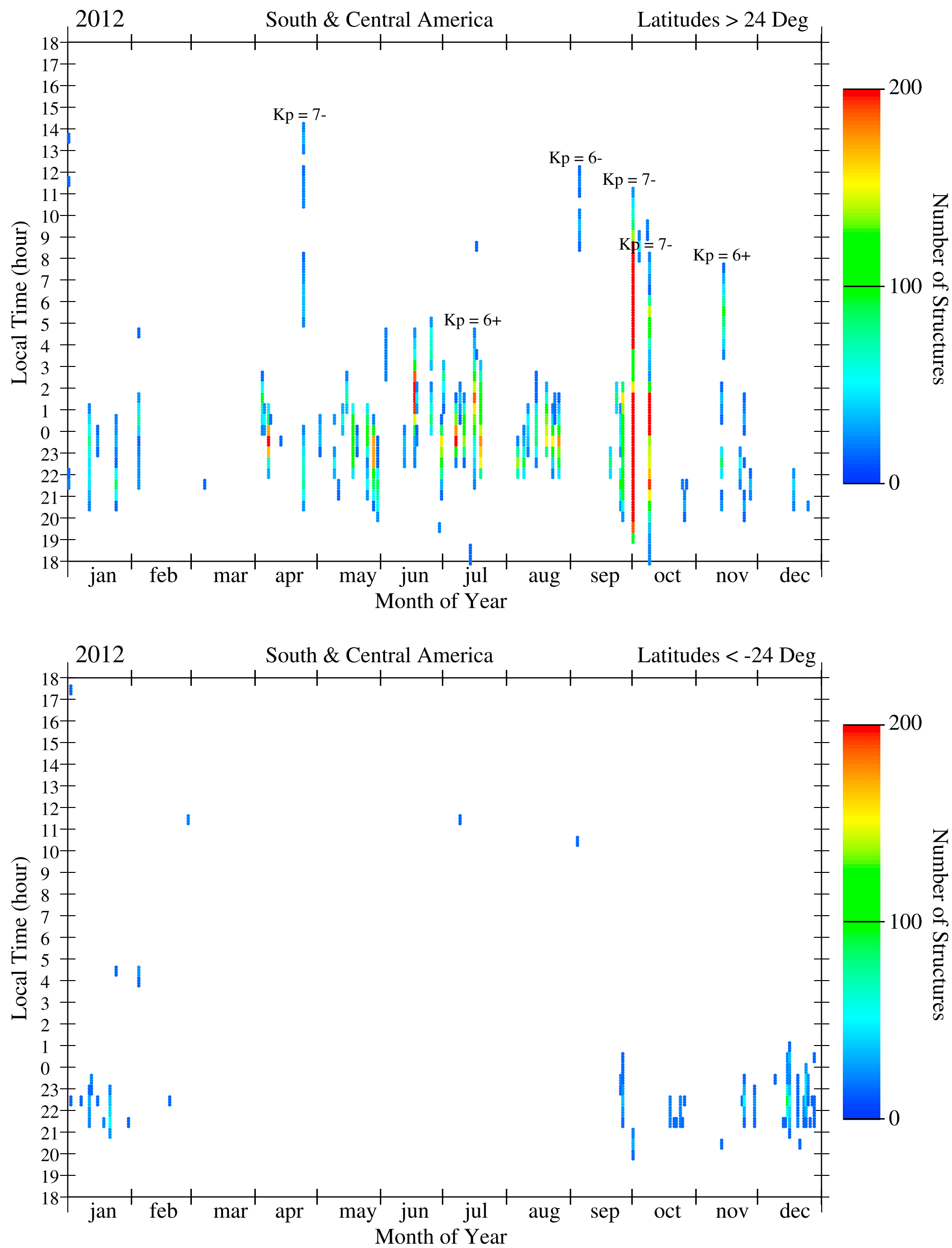

Figure 2. Total number of MSTID detections observed over Central America, the Caribbean region, and South America for every day of 2012. (top) Detections in the northern midlatitude regions (considered above 24° magnetic latitude). (bottom) Same as Figure 2 (top) but for the Southern Hemisphere (magnetic latitude below −24°).

MSTID. The station located farther north, Bermuda, does not show a significant TECP variation, but all the other stations display TECP values varying between 2 and 5 TECU. A group of 12 stations placed south of Bermuda and labeled 13 through 24 show TECP variations with peak amplitudes less than 2 TECU. In contrast, the stations labeled 1 to 12 display MSTIDs with higher amplitude and shorter periods. The station with the largest amplitude MSTID corresponds to Grenada (latitude = 12.2°, longitude = 61.6°W). In summary, TECP associated with nighttime MSTIDs were observed between Anegada, British Virgin Islands MLAT(MLAT = +27°), and Cumana in the northern coast of Venezuela (MLAT = +19°). Two hours before the onset of the MSTIDs, small-amplitude quasi-sinusoidal undulations were seen at the majority of the stations of Figure 3. These small TECPs can be interpreted as the signature of typical TIDs and likely associated with GWs.

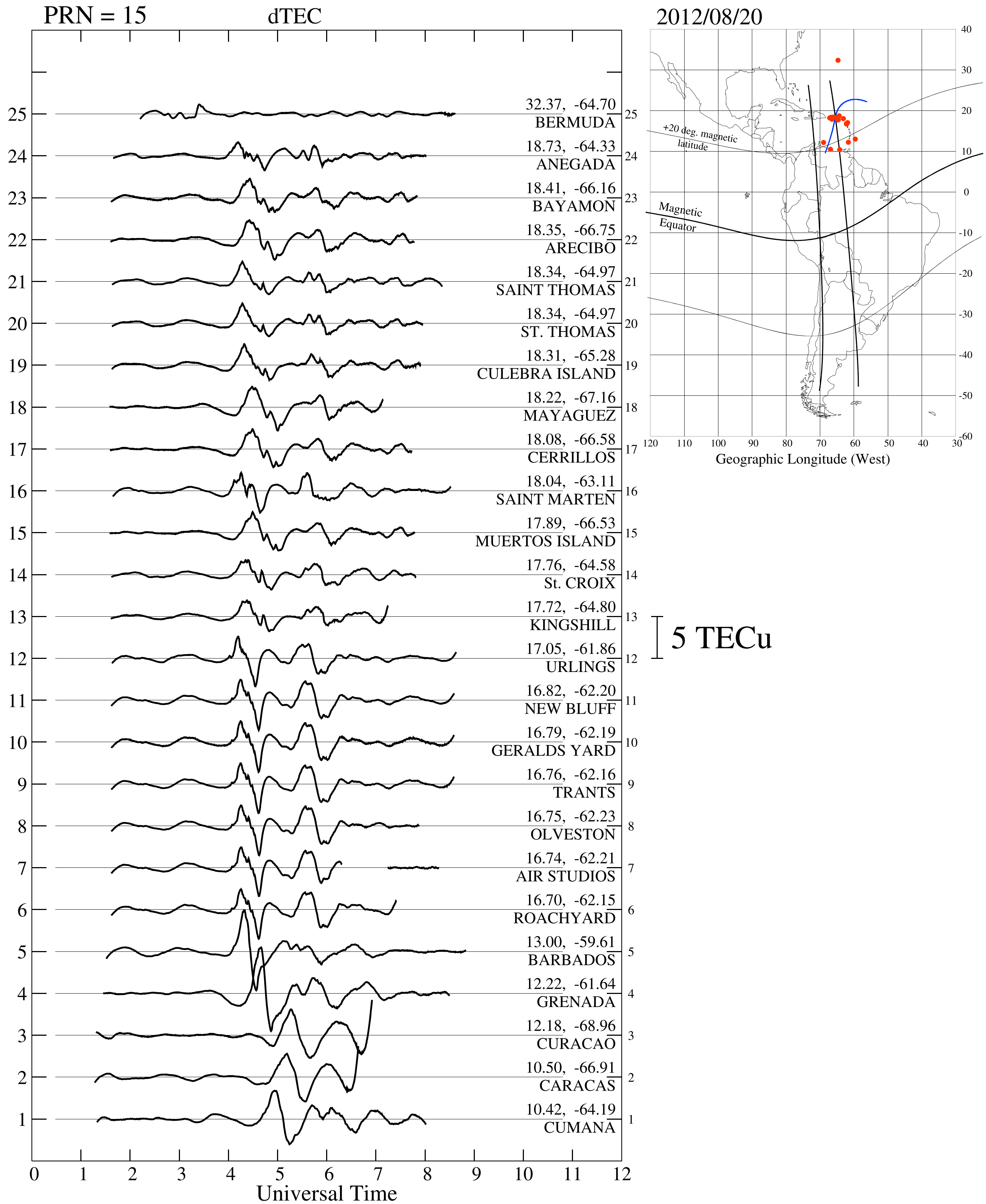

Figure 3. (left) TEC perturbation (TECP) values measured with 25 GPS receivers that are located in the Caribbean regions; (right) the receiver locations in red. Note that the scale used in this plot is equal to 5 TECU (total electron content unit, 1 TECU = 10^{16} el m^{-2}).

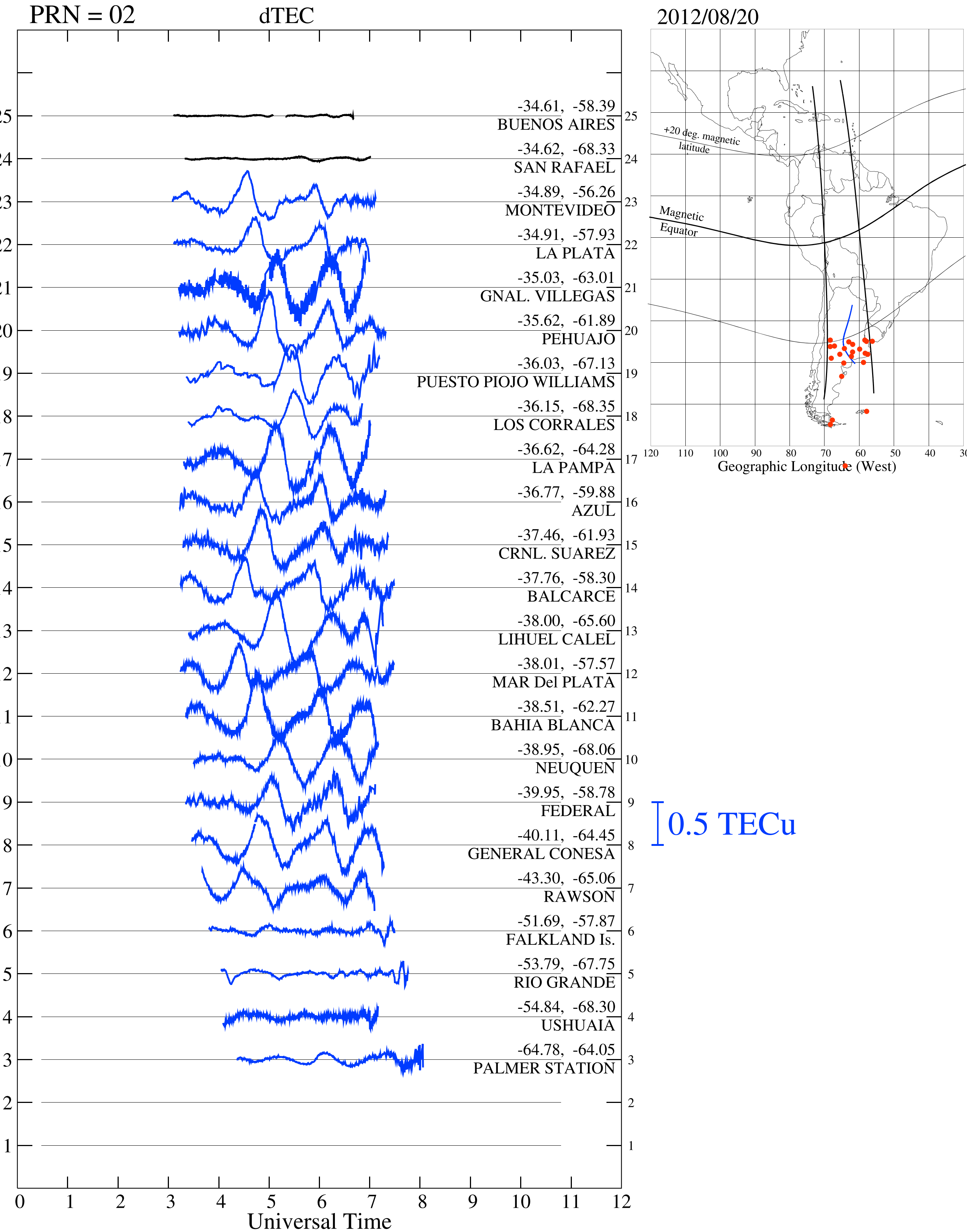

Figure 4. (left) Similar to Figure 3 but for TECP values measured in the Southern Hemisphere. (right) The location of the receivers near the southern end of South America. Note that the scale used in this plot is 10 times smaller (0.5 TECU) than the scale employed in Figure 3.

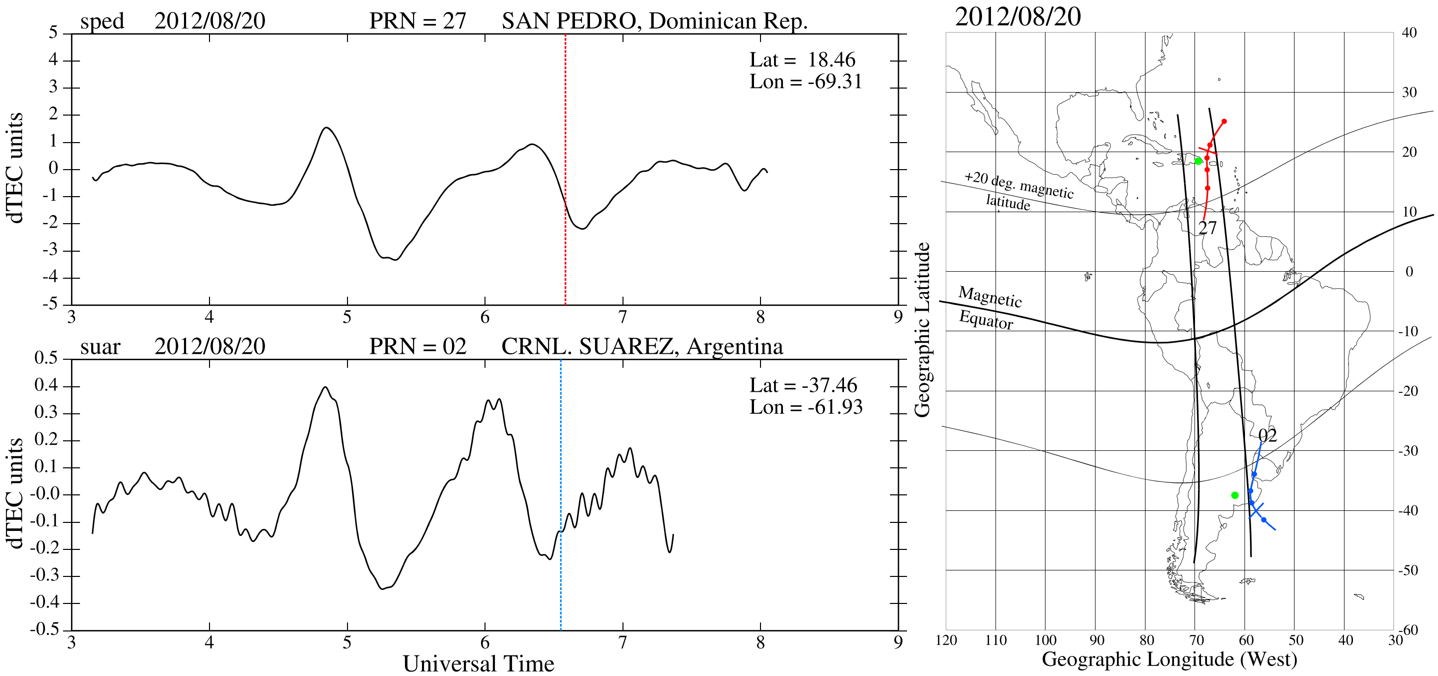

Figure 5. (left column) TECP values measured by receivers located (top) at San Pedro in the Dominican Republic and (bottom) at the conjugate location at Coronel Suarez in Argentina. (right) The locations of the stations (green dots) and the ionosphere piercing points from both stations.

Figure 3 (right) also includes the subionospheric intersection projections to the ground (in blue) as observed from the second station: Anegada. The following figures demonstrate that the MSTIDs of Figure 3 map to conjugate features in the Southern Hemisphere.

Figure 4 shows TECP traces associated with conjugated MSTIDs that were observed in the Southern Hemisphere over Argentina. Here the plot scale has been decreased by a factor of 10 (in blue) to visualize more fully the amplitude of the MSTIDs. It is also indicated that the background average TEC in the Southern Hemisphere is only 2 TECU compared to 10 units in the Northern Hemisphere. The geographic location of the 25 GPS receivers is indicated in Figure 4 (right) together with the ionospheric projection of the GPS satellite 02 from the San Rafael station (in blue). Figure 4 (left) shows the signature of a series of quasi-sinusoidal MSTIDs transiting between stations Montevideo in Uruguay (latitude = 34.9° S) and Rawson in Argentina (latitude = 43.3° S). Other stations located further north and others placed way south in Patagonia and in the Antarctica peninsula do not display TECP amplitudes larger than 0.3 TECU. It is important to note that a few stations in the Southern Hemisphere show MSTIDs starting ~10 min before the Northern Hemisphere counterparts. This apparent discrepancy about the timing of MSTIDs that appear in both hemispheres is due to the difference in the spatial coverage in both hemispheres and the fact that the MSTIDs likely originated over the Atlantic Ocean and entered the FOV of the GPS in the Southern Hemisphere much earlier than in the north. In the Southern Hemisphere the GPS FOV projects further east than in the Northern Hemisphere.

Figure 5 (left column) displays the TECP traces from two conjugate stations that simultaneously observed MSTIDs in opposite hemispheres. The geographic latitude and longitude of both stations are stated in each panel, and their locations are indicated in Figure 5 (right) by using large green dots. This panel also contains the trajectories of the subionospheric intersections for both northern (red) and southern (blue) passes, respectively. Hourly marks are indicated by red and blue dots along each of the trajectories. The GPS satellite number is also printed to denote the start of the pass. The scale of Figure 5 (bottom left) has been also reduced by a factor of 10 to help view the high degree of correlation and the similarity of the periodicity between both trains of MSTIDs. The peak amplitude of the northern MSTIDs is ~3 TECU compared to 0.4 TECU in the Southern Hemisphere. This implies a mapping factor, in TECU, equal to ~13%. However, it is noted that TEC is an integrated quantity and the mapping factor depends on the slant angle and does not quite represent the amount of density variability associated with the MSTIDs. In addition, as explained before and displayed

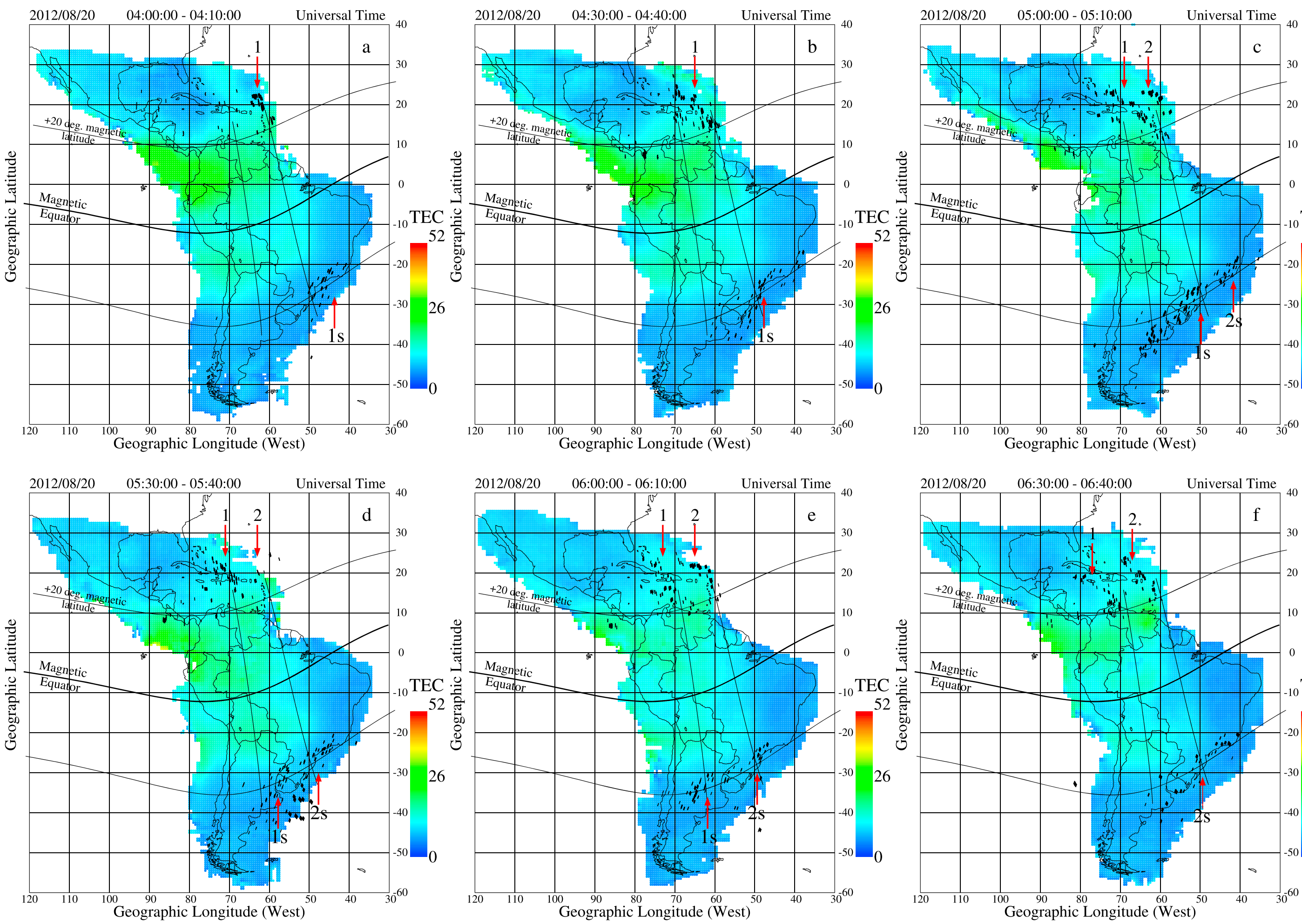

Figure 6. Sequence of regional maps of TEC values measured over South and Central America between 0400 and 0630 UT on 20 August 2012. The small black segments superimposed on the TEC maps illustrate negative TEC excursions due to the presence of MSTIDs at those locations.

in Figure 6, the background TEC is much reduced in the Southern Hemisphere due to seasonal and geographic effects. It is likely that the Southern Hemisphere contained a smaller peak density and the altitude of the *F* region was also reduced. All these factors probably contribute to the mapping characteristics and density variability in the opposite hemisphere. The red and blue lines near 06:30 UT indicate the times when the observations were the closest to conjugacy. It is also indicated that the bottom panel of Figure 5 also exhibits a 6 min period traveling ionospheric disturbance (TID) that seems superimposed on the conjugate MSTID.

The sequence of TEC images of Figure 6 display the evolution of the background TEC and the motion of the MSTIDs over Central America and the Caribbean region observed between 0400 and 0630 UT on 20 August 2012. The locations where MSTID are detected are displayed as short black segments superimposed on the TEC maps [*Valladares and Chau*, 2012]. As the magnitude of the TECP values are quite different in both hemispheres, different threshold values were used to display MSTIDs. We chose a threshold equal to 1.0 TECU for the Northern Hemisphere and 0.15 TECU for the Southern Hemisphere. Two magnetic field lines that intersect the magnetic equator at 65° and 55° W are drawn to point out the conjugate characteristics of the MSTIDs. Figure 6a shows a well-defined anomaly with a dominant northern crest. During the following 2.5 h the ionosphere undergoes the typical nighttime decrease, the northern crest of the anomaly persists, and the southern crest becomes diffuse and practically recombines. Figure 6a marks the time when the MSTID labeled 1 (red arrow) enters the area probed by the Northern Hemisphere GPSs. In the Southern Hemisphere the extension of the MSTID, labeled 1s, is much larger due to the more extensive coverage of the GPS receivers in the Southern Hemisphere. Figure 6b denotes the westward motion of MSTID 1 to a

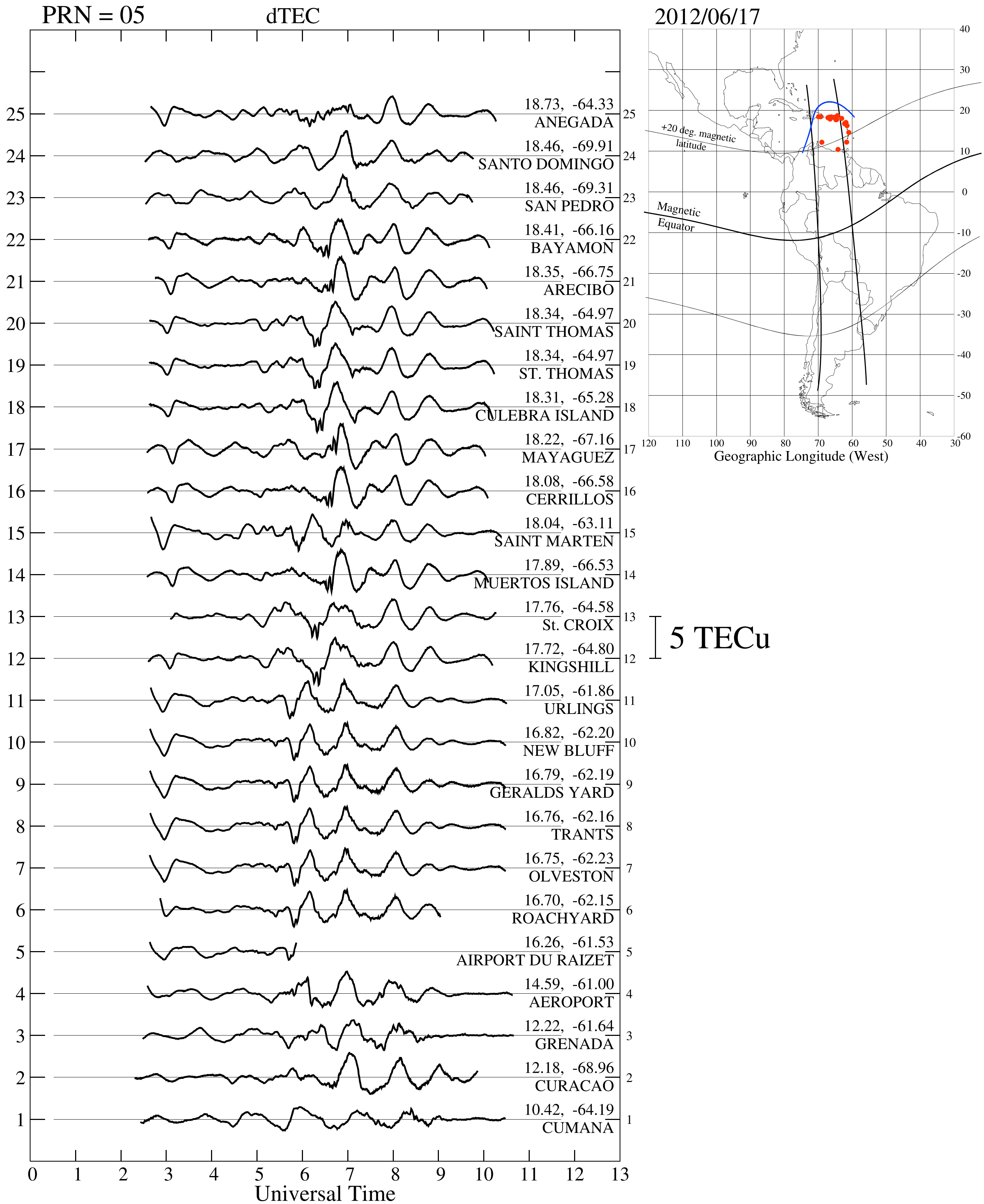

Figure 7. Similar to Figure 3 but corresponding to 17 June 2012 and for the Northern Hemisphere.

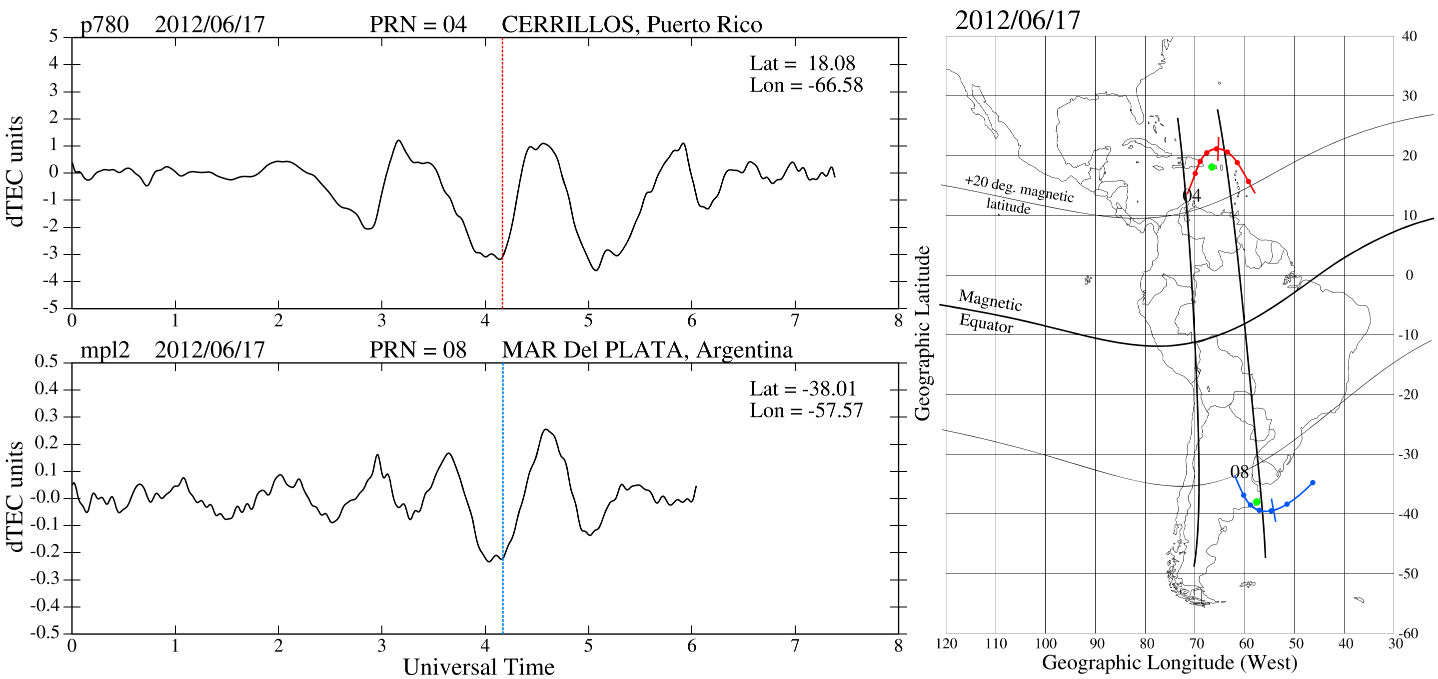

Figure 8. Similar to Figure 5 but corresponding to 17 June 2012. (left column) Measurements at Cerrillos in Puerto Rico and Mar del Plata in Argentina.

new location placed ~300 km apart. The corresponding westward drift is also seen in the Southern Hemisphere, and the full extension of the MSTID is captured indicating a length equal to ~1500 km. Figure 6c presents TEC and MSTID information obtained between 0500 and 0510 UT. This figure displays the entrance of a second MSTID, named 2 and 2s, in the Northern and Southern Hemispheres, respectively. Similar to MSTID 1, the second MSTID seems to have originated further east of the GPS FOV in the American continent. Figure 6c also gives evidence that MSTID 1 has continued moving westward and that the northern end of the MSTID is located over Puerto Rico and the conjugate MSTID along the western Coast of South America. Figures 6d–6f confirm that both MSTIDs continue moving westward during the following 90 min. However, their velocity does not seem to remain constant during this period. The separation between the MSTIDs has also increased from a value close to 700 km in Figure 6b to more than 1000 km in Figure 6f. Figure 6e shows MSTID 1 being affected by a Y-forking feature that occurs near 0600 UT. A movie showing the evolution and transit of the MSTIDs has been included in the supporting information.

2.2. MSTIDs Observed on 17 June 2012

The geomagnetic conditions during the first 6 h of 17 June 2012 were moderately active with the *Kp* index equal to 4− and 3+. During the following 6 h the *Kp* index rose to 6^0 due to the onset of a magnetic storm. On this day, MSTIDs started after 03 UT and lasted for ~7 h. The MSTIDs had large widths, occupying a larger area that spanned into the Central America region. Figure 7 shows TECP values measured at 25 stations using GPS signals from satellite 05. The format of this figure is similar to that of Figure 3. However, here there exists a long succession of positive and negative excursions typical of TEC fluctuations associated with MSTIDs. Figure 7 also shows an event of relatively rapid TEC fluctuations that are simultaneously observed at several stations between 06 and 07 UT. It is important to mention that similar to the event of 20 August 2012, TEC depletions associated with plasma bubbles were not detected by the GPS receivers operating in South America.

Figure 8 shows the conjugate characteristics of TECP values recorded at two conjugate stations: Cerrillos in Puerto Rico and Mar del Plata in Argentina. The GPS satellite trajectories are also drawn in Figure 8 (right) to point out the symmetry and conjugacy between these two passes. Due to the special geometry of the satellite passes, the peaks and valleys of the TECP curves are closely aligned after 3 UT when MSTIDs start developing in the Caribbean region. The amplitude of the TECP was close to 3 TECU in Puerto Rico, but they

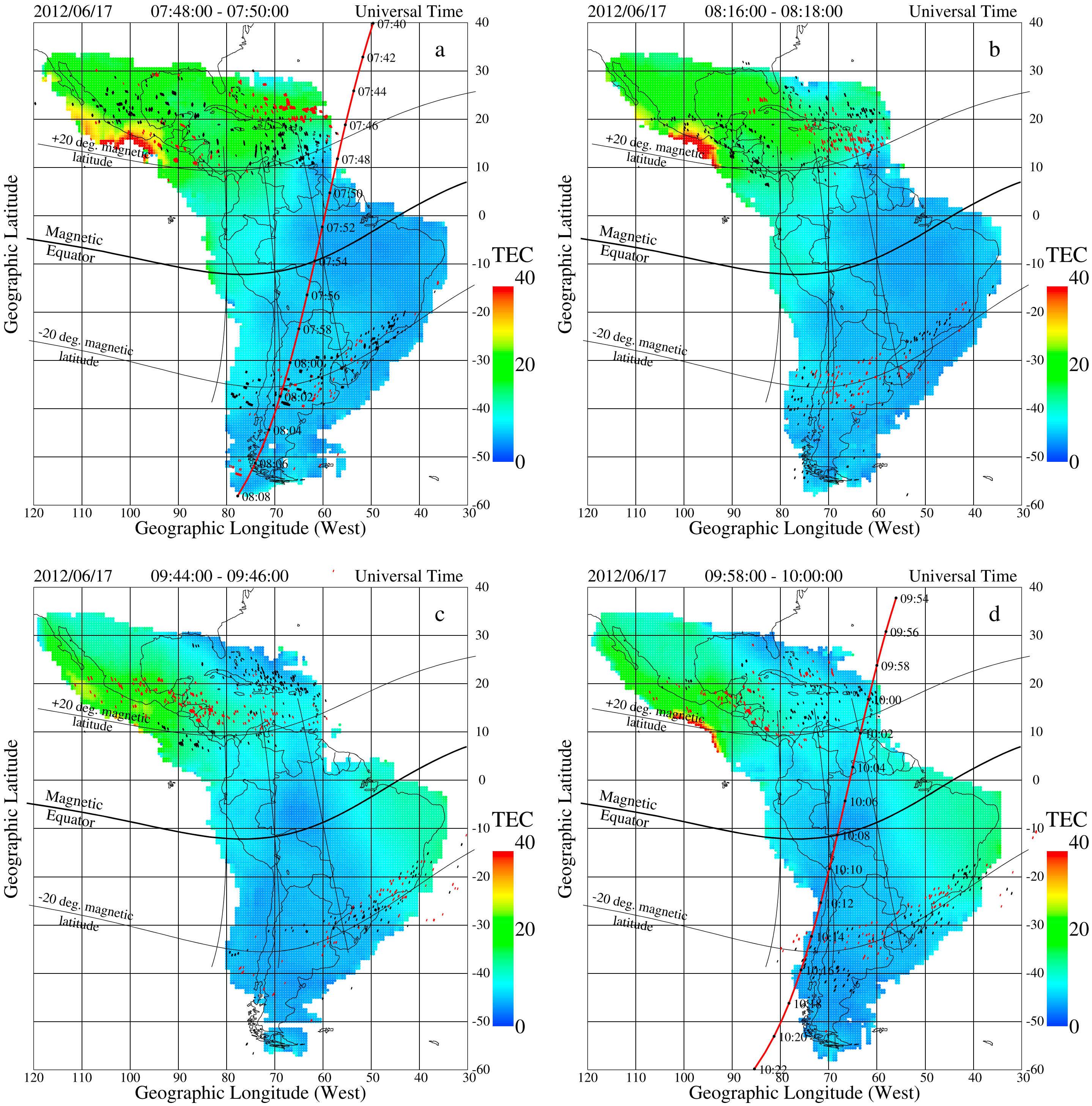

Figure 9. Similar to Figure 6 but for TEC values and MSTID structures observed on 17 June 2012. Time intervals for different frames are (a) 0748–0750 UT, (b) 0816–0818 UT, (c) 0944–0946 UT, and (d) 0958–1000 UT. The satellite tracks correspond to DMSP-F15 in Figure 9a and DMSP-F17 in Figure 9d.

were not larger than 0.25 TECU at the conjugate location in Mar del Plata. This signifies a TEC mapping factor equal to 8.3%.

Figure 9 displays selected images of the background TEC values observed on 17 June 2012. The format of this figure is similar to that of Figure 6, in addition, short red segments are introduced to indicate locations where positive (e.g., enhanced) TEC fluctuations occur. Figures 9a–9d portray the temporal evolution of TEC and

TECP associated with a series of MSTIDs that developed during the initial phase of the magnetic storm of 17 June 2012. Figures 9a and 9d correspond to the times when two DMSP satellites (F15 and F17) passed across the Caribbean region and were able to measure the *F* region topside above the MSTIDs. The DMSP density measurements are presented in section 4. Figure 9a shows a series of wide positive-negative bands that extend for several degrees in latitude and seem to be aligned 25° north from geographic west. Figure 9b, obtained 28 min later, shows the presence of well-defined bands of enhanced and then depleted regions near the eastern part of the Caribbean region. Close comparison of Figures 9a and 9b suggests that the red bands have drifted westward for a few hundreds of kilometers and is seen between the field lines that cross the magnetic equator at 70° and 60°W. This band maps to another wide band of enhanced densities (e.g., "red" segments) in the Southern Hemisphere. There also exists a band of decreased TEC or black segments over the Central America region. During the event of 17 June 2012, the amplitude of the MSTIDs varies between 0.5 and 3 TECU in the Northern Hemisphere. However, in the Southern Hemisphere, MSTIDs deviate between 0.1 and 0.25. It is noted that we are using 0.1 TECU as the minimum threshold for TID detection to prevent any false TID detection. Figure 9c shows that the "red" band has drifted further poleward and is placed above Central America. Figure 9d displays an absence of MSTIDs over the Caribbean region except for the red band that is about to exit the FOV of the GPS receivers through the western coast of Central America. Comparison of both events presented in this section indicates that the MSTIDs of 17 June 2012 were considerably more dynamic, and the peaks and valleys were much wider, extended for longer distances, and persisted for a few more hours.

3. Multistation Analysis of MSTID Phase Velocity

This section describes the calculation of the MSTID phase velocity using the TEC perturbation values observed on 20 August 2012. The analysis is basically restricted to the MSTIDs seen over the Caribbean region and at their conjugate locations in South America. The analysis is based on the algorithm described by *Valladares and Hei* [2011] and *Valladares and Chau* [2012]. This algorithm was originally developed to derive the phase vector of TIDs using TEC values collected by three stations separated by tens of kilometers or less. Here the method has been generalized and applied to TEC data from multiple (more than four) stations. Obviously, it is necessary that the same MSTID is detected by all the different GPS receivers.

In essence, the algorithm is based on performing multiple cross correlations and employing the formula of the phase velocity equation given by $V \times \tau_i = Y_i \cos(\alpha) + X_i \sin(\alpha)$. Here V is the MSTID phase velocity; τ_i is the time delay of the TECP traces between the ith and an adjacent station; X_i and Y_i are the longitudinal and latitudinal distances between the subionospheric projections at times t and $t + \tau_i$ in a Cartesian coordinate system; and α is the propagation direction of the MSTID and considered clockwise and a value equal to zero at geographic south. It is indicated that the velocity calculation is based on the assumption that the MSTID phase velocity is constant during the analysis time interval. Nevertheless, other less stringent constraints can be selected by subdividing the stations into two or more groups or assuming a linear or square variability of the velocity.

3.1. Northern Hemisphere Observations

Figure 10a shows the TECP values observed at 22 stations within the Caribbean region. The small Figure 10b displays the location of the stations in red and the subionospheric projections in blue. A larger blue dot is also used to indicate the beginning of the northward directed passes. It is evident that all the traces in Figure 10a have a high degree of coherence. Visual inspection indicates a positive delay for most of the adjacent traces. The stations were originally arranged according to their latitude and starting with the most northward station at the top and then progressing toward the most southern station at the bottom. However, it was found later that on this day the MSTIDs propagated in a slant path (SW direction). Therefore, the plotting of the TECP traces was not arranged from north to south, but in a direction that has a slant angle of 40° clockwise from south. The latitude, longitude, and the four-letter name of the station is printed on the right margin of the plot. Figure 10c shows the cross correlation functions obtained after correlating the TECP traces for each set of two adjacent stations. The short vertical red segments indicate the time delay between the stations. Figure 10d presents the results of the velocity analysis. The small open circles have been color coded to represent the time delay gathered in the correlation analysis with red meaning longer delays and blue circles pointing out delays close to zero. The small vector at the center of the circles indicates the magnitude and

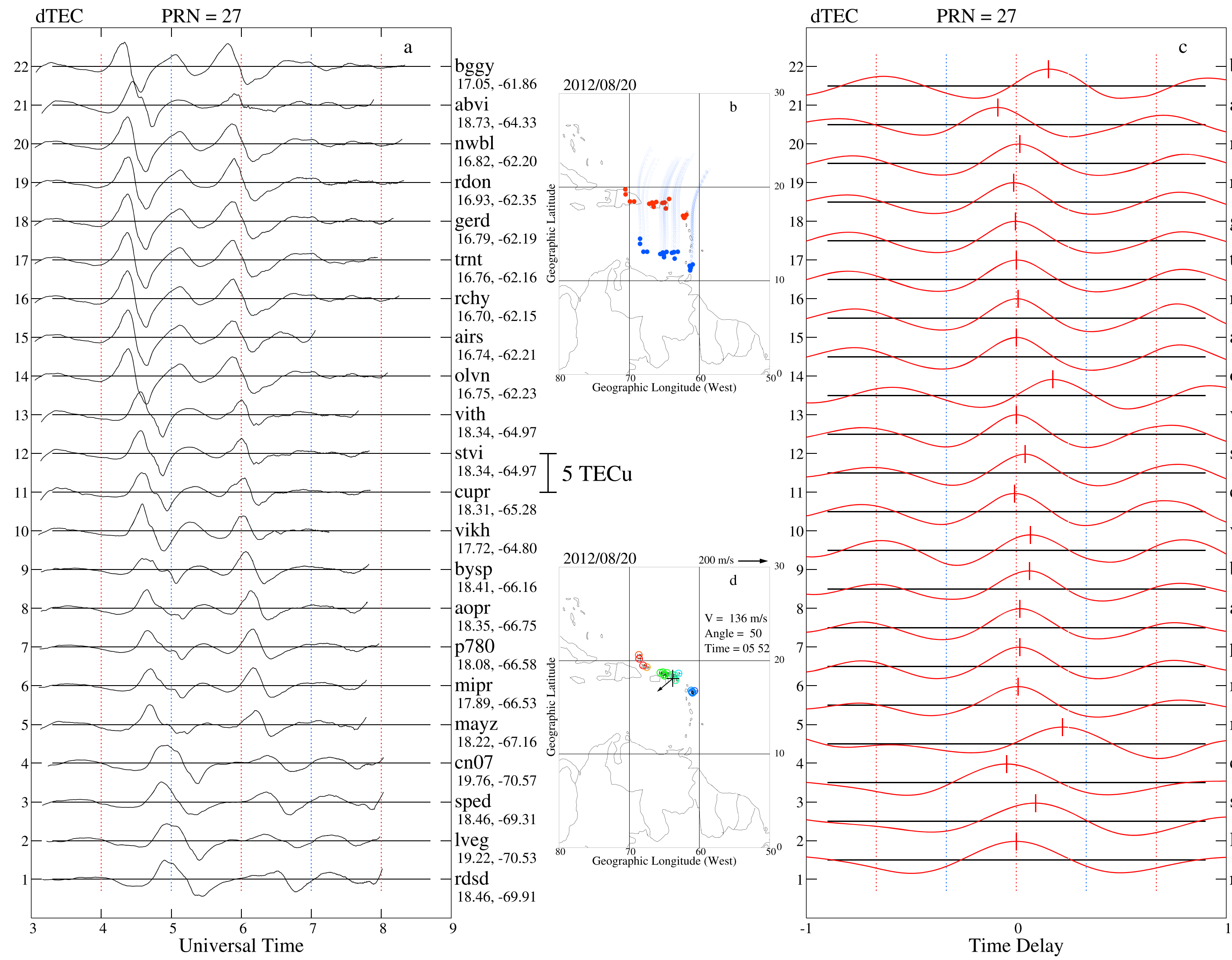

Figure 10. Full analysis of the amplitude and propagation direction of the Northern Hemisphere MSTIDs of 20 August 2012. (a) TECP traces for 22 stations in the Caribbean region. (b) Ionospheric intersection points and location of 22 stations. (c) Cross-correlation functions between adjacent TECP traces. (d) Arrow representing the MSTID vector velocity.

direction of motion of the MSTIDs. We found a phase velocity equal to 138 ± 11 m/s that was directed 50° west from south.

Figure 11 exhibits the spatial/temporal variability of the phase velocity derived between 03 and 06 UT. During these times the Northern Hemisphere MSTIDs crossed the FOV of the Caribbean GPS receivers. The length and direction of the arrows point out the magnitude and angle of propagation of the nighttime MSTIDs. Color indicates the UT hour when velocities were observed and varies between 02 UT in blue and 06 UT in red. The common feature on 20 August 2012 is the fact that all vectors point near 60° clockwise from south. Over the Caribbean region, the magnitude of the MSTID velocity varies between 350 ± 29 m/s at 3 UT and 140 ± 15 m/s at 05 UT. In the northern part of South America, a value near 200 ± 18 m/s was observed. These values are larger than the phase velocities of band-like structures discussed by *Behnke* [1979], who found speeds below 60 m/s. *Garcia et al.* [2000] conducted more extended observations to demonstrate that the MSTID velocity can vary between 50 and 170 m/s. The larger MSTID velocity may be due to the storm conditions that prevailed during the nighttime MSTID event containing very rapid seeds. In addition, we have been able to follow the velocity of the MSTIDs for several hours from their initiation when the MSTIDs were moving very fast until their decay when they move with much slower velocities across the Arecibo observatory in Puerto Rico. These results are evident in Figure 11.

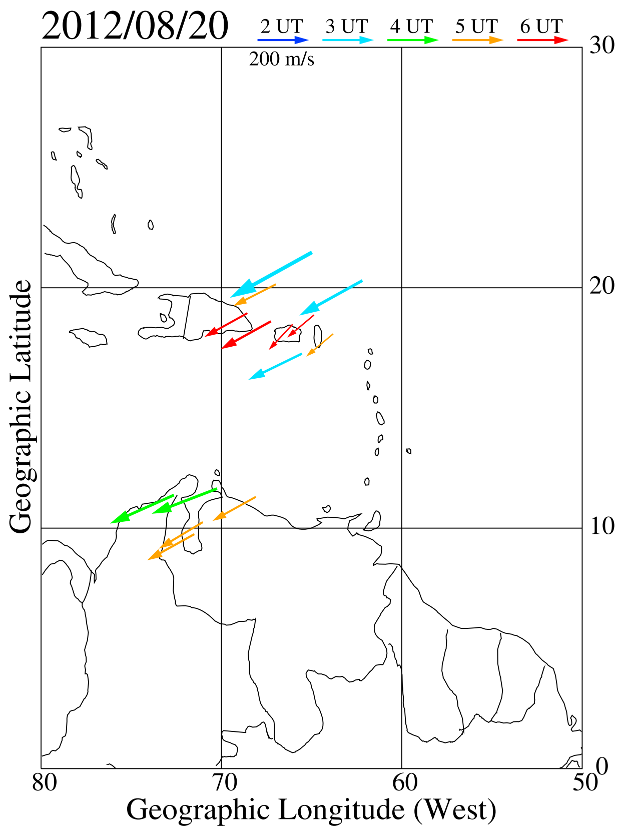

Figure 11. Geographic plot displaying the time-space variability of the MSTID variability during the night of 20 August 2012. The colors of the arrows indicate the time of the velocity measurements as indicated at the top.

3.2. Southern Hemisphere

Figure 12 displays the analysis of the TECP values gathered from receivers placed at the conjugate locations in the Southern Hemisphere in a format similar to Figure 10. Figure 10a shows the TECP values for 12 stations placed in the northeastern part of Argentina and Uruguay. Figures 10b and 10c display the station locations, the satellite subionospheric intersection from each station, and the correlation functions. Figure 10d shows the result of the velocity analysis in which we obtained a velocity equal to 198 ± 15 m/s directed northwest (123° from south). This direction of the phase velocity is in agreement with previous measurements of the conjugate motion of MSTIDs conducted with imagers [*Shiokawa et al.*, 2005; *Martinis et al.*, 2011]. The magnitude of the velocity is about 60 m/s larger than the speed measured in the Northern Hemisphere (Figure 10) that corresponds to 1 h later. This difference may be explained by the temporal variability of the MSTID speed, as shown in Figure 11, or due to differences between the Northern and Southern Hemisphere magnetic fields of the Earth. According to the International Geomagnetic Reference Field (IGRF) model, the magnitude of the magnetic field is 30% less in the Southern Hemisphere that in the northern side. It is also worth mentioning that several of the TEC traces of Figure 12a display the "6 min" oscillation that was seen in Figures 5 and 8.

4. DMSP Observations

On 17 June 2012 two DMSP satellites (F15 and F17) passed over the Caribbean region during the observations of the nighttime MSTIDs. These two satellites are in a near-circular, Sun-synchronous, polar orbit at 840 km altitude. The DMSP-F15 satellite was launched in 1999 and orbits on the local time meridian between 09 and 21 LT. DMSP-F17 was launched in November 2006. On 17 June 2012 the satellites traversed the FOV of the GPS receivers from north to south as seen in Figures 9a and 9d. These figures display the satellite tracks to help the reader to relate the density perturbations measured in situ (Figure 13) and the TEC perturbations observed on the ground (Figure 9).

Figures 13a and 13b show the density variability obtained by subtracting a running average of 2 min to every 1 s density value. This method allows us to remove density variations with scale sizes larger than 900 km and display density variability containing higher frequency. A comparison of Figure 13a and the satellite tracks in Figure 9 indicates that DMSP-F15 crossed above the negative excursion of TEC, between 0746 and 0748 UT. During this time a positive density variability as high as 10^4 cm^{-3} is seen in Figure 13a. A closer comparison between the satellite and the ground observations was conducted mapping the DMSP observations at 840 km down to 350 km altitude using the IGRF12 model of the field lines. At 0747 UT, the DMSP-F15 satellite is located at latitude = 15°, longitude = 56°W and altitude = 840 km. This location maps to latitude = 18°, longitude = 57.3°W at 350 km. One minute later, at 0748 UT, the DMSP-F15 satellite is moving across latitude = 12°, longitude = 57°W, altitude = 840 km. This location maps to latitude = 16°, longitude = 58.4°W at 350 km altitude. Figure 9a confirms that the latitude band between 18° and 16° corresponds to a region of negative

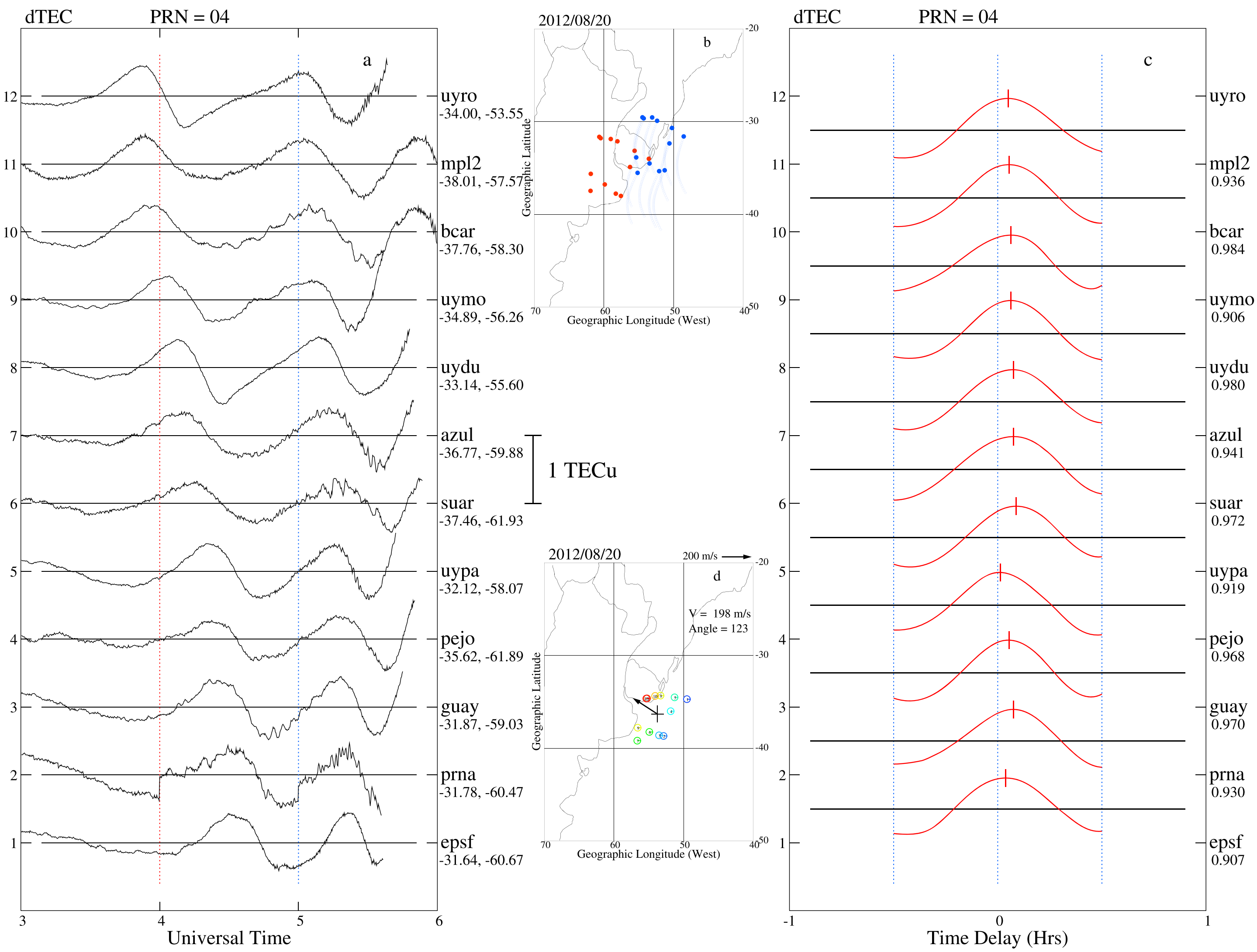

Figure 12. Similar to Figure 10 but corresponding to the MSTIDs observed in the Southern (conjugate) Hemisphere on 20 August 2012.

TEC perturbations (e.g., black dots). Therefore, an anticorrelation exists between TECP and the density variability at the *F* region topside measured by DMSP-F15. During the following minute, 0748–0749 UT, the in situ density decreases by $10^4\,cm^{-3}$. However, we did not obtain a clear signature of the presence of MSTIDs in that region. We believe that a MSTID population extended into the northern part of South America but was not detected as we kept a high detection threshold (1 TECU) for MSTIDs in the Northern Hemisphere.

Figure 13b shows the density variability measured by DMSF-17 that crossed over a region of negative TEC excursions between 1000 and 1002 UT. During these two minutes another region of increased density is seen in the satellite data. The anticorrelation between GPS TECP and the in situ density variability endorses the view that the MSTIDs of 17 June 2012 correspond to rising and falling sheets of plasma. These measurements support our contention that the TECPs displayed in Figure 9 are MSTIDs that are electrified and map to the MSTIDs seen in the southern conjugate hemisphere (Figure 8).

5. Discussion

This paper has shown the characteristics of nighttime midlatitude MSTIDs observed in the American sector on 20 August 2012 and 17 June 2012. On 20 August 2012 MSTIDs, also named electrobuoyancy waves, last for at least 3 h; they map to the opposite conjugate hemisphere and move with phase velocities varying

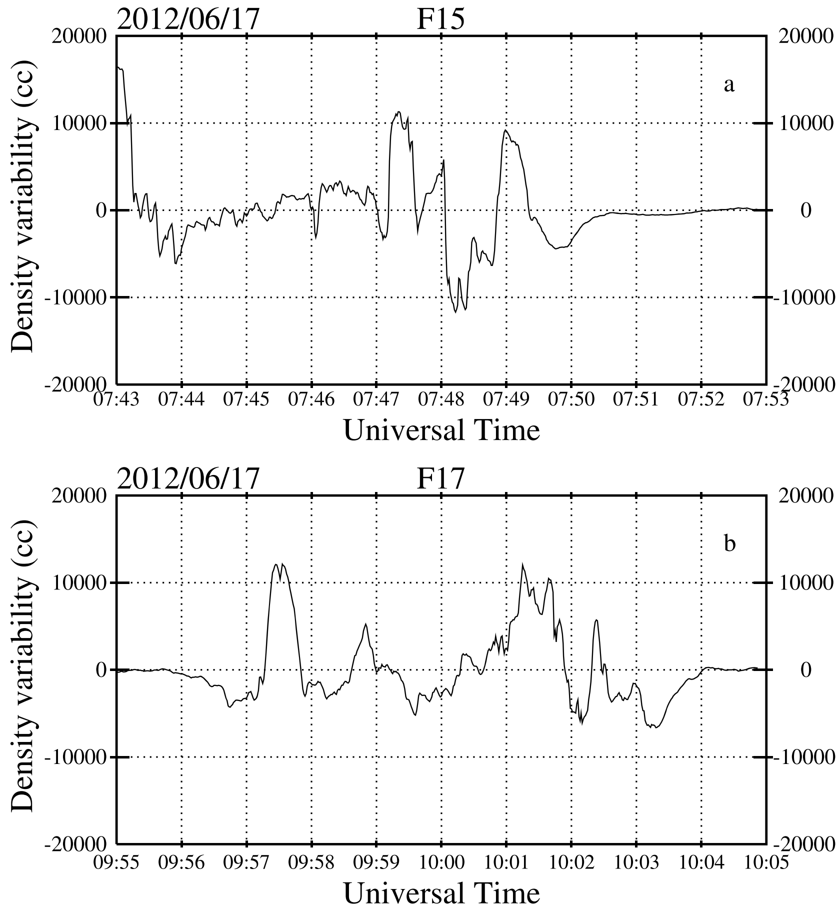

Figure 13. Plots of the density variability measured by two DMSP passes on 17 June 2012 after subtracting a 2 min running mean. (a) DMSP-F15 and (b) DMSP-F17.

between 140 and 350 m/s. We found that the velocity directions were almost constant through the night. In terms of TECP values, we measured a mapping ratio of 13% between the Northern and Southern Hemispheres on 20 August 2012 and 8% on 17 June 2012. On 20 August 2012 the background TEC was 10 TECU in the Northern Hemisphere and only 2 TECU in the Southern Hemisphere. On 17 June 2012 the values were 20 and 3 TECU for the Northern and Southern Hemispheres, respectively. We believe that the large differences in the background density and the variability of *F* region altitude between hemispheres produce the large asymmetry in the amplitude of the TEC perturbation. Figures 6 and 9 demonstrated that the separation between successive peaks of the MSTID train can vary between 700 and 1200 km. These figures also indicated that the length of the MSTIDs along their major axis can be as large as 2000 km. This value is in accord with measurements presented by *Tsugawa et al.* [2007]. The GPS TEC values have demonstrated that the MSTIDs observed on these two days exhibit conjugate characteristics. However, we cannot conclude that all TIDs map to the opposite hemisphere; it would be necessary to perform the velocity analysis described in section 3.

Miller et al. [1997] and *Kelley and Miller* [1997] have suggested that thermospheric gravity waves can seed the Perkins instability. Their conceptual model included gravity waves that raise and/or lower the ionosphere to perturb the local conductivity, create a divergence of the current, and generate electric fields that could seed the Perkins instability. They stressed that the perturbations should be oriented in a direction for which the Perkins growth rate was larger. Our analysis concluded that on 20 August 2012 the direction of motion was practically constant during ~3 h and the MSTID phase velocity decayed from 340 m/s to less than 150 m/s. Based on this, we put forward the notion that on 20 August 2012 a train of GWs moving in a direction 50° from south was able to seed MSTIDs that slowed down with time as the seeding mechanism faded.

We do not have complete information on the activity of E_s layers on both hemispheres, and we cannot rule out the possibility that an E_s layer excited the Perkins instability as described by *Cosgrove and Tsunoda* [2004] and *Cosgrove et al*. [2004]. Nevertheless, the digisonde at Ramey in Puerto Rico did not observe E_s layers on August 20 2012 and only between 07 and 8 UT on 17 June 2012. It will be also necessary to have another ionosonde placed in the Southern Hemisphere to fully address the role of E_s layers on seeding the Perkins instability. A new VIPIR ionosonde has been operating at Tucuman in Argentina since October 2014. We plan to include valuable information from this system in future investigations.

Figure 2 points out the role of magnetic activity on the production of MSTIDs. This Figure suggests that during storms, when the *Kp* index is equal to 6+ or higher, MSTIDs persist for longer hours and populate higher latitudes (not shown). We also indicate that an average of 15 nights per year have large MSTID events that last for a few hours. There are also 10 events per year when equatorial plasma bubbles extend up to high altitudes and TEC perturbations reach magnetic latitudes above 24°. These cases could be mistaken for MSTIDs if no calculation of their motion is carried out or no observations are performed at lower magnetic latitudes. The large coverage of the LISN distributed observatory and the analysis software that has been developed overcomes both deficiencies. There also exists about six cases per year—in 2012—of MSTIDs extending to much higher magnetic latitudes (>40°) that occur during super storms. All these cases have not been addressed here and will be the subject of further investigations. At the present time we have TEC data for years 2010–2015 that make a total of ~100 cases for MSTID that originated in the Northern Hemisphere and a smaller number for the Southern Hemisphere. This is a superb database that will be mined and complemented with passes of C/NOFS, DMSP, and SWARM satellites. Satellite measurements provide the density variability in the opposing hemisphere when no TEC values are available. In addition, satellites near Earth are able to measure the electric and magnetic fields that can confirm the existence of mapping fields due to the generation of the electrified buoyancy waves/MSTIDs. Maps of TEC perturbations will be used to investigate whether or not gravity waves, especially the fast-moving waves, are seen prior to the initiation of MSTIDs. The analysis of a large number of events will make it possible to discern if gravity wave seeding is the dominant mechanism of MSTID formation.

6. Conclusions

This study has led to the following conclusions:

1. TEC values measured with several networks of GPS receivers that operate in the American sector were used to investigate the spatial variability and dynamics of nighttime MSTIDs that occur at these longitudes. This valuable and rich data set of TEC values was exploited using a refined processing technique that extracted parameters associated with the dynamics and conjugacy of the nighttime MSTIDs. It is also concluded that networks of GPS receivers offer a cost-effective method to follow MSTID dynamics across the American continent and in both hemispheres.
2. Both nighttime MSTID events shown in this study presented conjugate structures that developed in both hemispheres. It seems that both events originated in the Northern Hemisphere as the TEC, and consequently, the number density is higher at that location. Both TEC and TECP values were quite different in the two hemispheres. The discrepancy in the background TEC between hemispheres is likely due to seasonal changes as both days are close to the summer (Northern Hemisphere) solstice. The TEC ratio between hemispheres was equal to 5 and the TECP ratio of order 10%. More studies are needed to address events when the MSTID originates in the Southern Hemisphere.
3. The MSTID phase velocity was directed SW in the Northern Hemisphere and NW in the Southern Hemisphere. They perfectly mirror each other. On 20 August 2012 the MSTID velocity decreased from 350 m/s to 140 m/s during a 3 h time interval; however, the propagation direction remained constant during the observation period.
4. Density variability measured by two DMSP satellites during the MSTID of 17 June 2012 indicated the presence of enhancements and depletions when crossing regions close to the MSTIDs. This fact suggested the presence of rising and falling sheets of ionization and the role of a Perkins-type instability on creating polarization electric fields to move ionospheric profiles.
5. It was postulated that a train of GWs circulated in the Caribbean region and seeded the onset of the MSTIDs. Further work is needed to investigate the necessary ionospheric and wave conditions that favor the development of the nighttime MSTIDs.

Acknowledgments
The authors would like to thank Claudio Brunini and Mauricio Gende of the Geocentric Reference System for the Americas (SIRGAS) and Michael Bevis from Ohio State University-Central and Southern Andes GPS Project (OSU-CAP) for providing GPS data that were used in this study. Hector Mora from the Colombian Institute of Geology and Mining (INGEOMINAS) provided RINEX files from several stations in Colombia. One of the authors, C.E.Valladares, was partially supported by Air Force Research Laboratory contract FA8718-09-C-0041 and NSF grants ATM-1135675 and ATM-1242476. The Low-Latitude Ionospheric Sensor Network (LISN) is a project led by Boston College in collaboration with the Geophysical Institute of Peru and other institutions that provide information for the benefit of the scientific community. We thank all organizations and persons that are supporting and operating receivers in LISN. The TEC values presented in this publication are stored in the LISN web page (http://lisn.igp.gob.pe).

References

Behnke, R. A. (1979), *F* layer height bands in the nocturnal ionosphere over Arecibo, *J. Geophys. Res.*, *84*, 974–978, doi:10.1029/JA084iA03p00974.

Burnside, R. G., J. C. G. Walker, R. A. Behnke, and C. A. Gonzales (1983), Polarization electric fields in the nighttime *F* layer at Arecibo, *J. Geophys. Res.*, *88*, 6259–6266, doi:10.1029/JA088iA08p06259.

Choi, H.-S., H. Kil, Y.-S. Kwak, Y.-D. Park, and K.-S. Cho (2012), Comparison of the bubble and blob distributions during the solar minimum, *J. Geophys. Res.*, *117*, A04314, doi:10.1029/2011JA017292.

Cosgrove, R. B. (2002), A direction-dependent instability of sporadic-*E* layers in the nighttime midlatitude ionosphere, *Geophys. Res. Lett.*, *29*(18), 1864, doi:10.1029/2002GL014669.

Cosgrove, R. B. (2004), Coupling of the Perkins instability and the sporadic-*E* layer instability derived from physical arguments, *J. Geophys. Res.*, *109*, A06301, doi:10.1029/2003JA010295.

Cosgrove, R. B., and R. T. Tsunoda (2004), Instability of the *E–F* coupled nighttime midlatitude ionosphere, *J. Geophys. Res.*, *109*, A04305, doi:10.1029/2003JA010243.

Cosgrove, R. B., R. T. Tsunoda, S. Fukao, and M. Yamamoto (2004), Coupling of the Perkins instability and the sporadic E layer instability derived from physical arguments, *J. Geophys. Res.*, *109*, A06301, doi:10.1029/2003JA010295.

Duly, T. M., N. P. Chapagain, and J. J. Makela (2013), Climatology of nighttime medium-scale traveling ionospheric disturbances (MSTIDs) in the central Pacific and South American sectors, *Ann. Geophys.*, *31*, 2229–2237, doi:10.5194/angeo-31-2229-2013.

Fukao, S., M. C. Kelley, T. Shirakawa, T. Takami, M. Yamamoto, T. Tsuda, and S. Kato (1991), Turbulent upwelling of the midlatitude ionosphere: 1. Observational results by the MU radar, *J. Geophys. Res.*, *96*, 3725–3746, doi:10.1029/90JA02253.

Fukushima, D., K. Shiokawa, Y. Otsuka, and T. Ogawa (2012), Observations of equatorial nighttime medium-scale traveling ionospheric disturbances in 630-nm airglow images over 7 years, *J. Geophys. Res.*, *117*, A10324, doi:10.1029/2012JA017758.

Garcia, F., M. Kelley, J. Makela, and C.- S. Huang (2000), Airglow observations of mesoscale low-velocity traveling ionospheric disturbances at midlatitudes, *J. Geophys. Res.*, *105*, 18,407–18,415, doi:10.1029/1999JA000305.

Hanson, W. B., and F. S. Johnson (1992), Lower midlatitude ionospheric disturbances and the Perkins instability, *Planet. Space Sci.*, *40*, 1615–1630.

Kelley, M. C., and S. Fukao (1991), Turbulent upwelling of the mid-latitude ionosphere: 2. Theoretical framework, *J. Geophys. Res.*, *96*, 3747–3753, doi:10.1029/90JA02252.

Kelley, M. C., and J. J. Makela (2001), Resolution of the discrepancy between experiment and theory of midlatitude *F*-region structures, *Geophys. Res. Lett.*, *28*, 2589–2592, doi:10.1029/2000GL012777.

Kelley, M. C., and C. A. Miller (1997), Electrodynamics of midlatitude spread *F* 3. Electrohydrodynamic waves? A new look at the role of electric fields in thermospheric wave dynamics, *J. Geophys. Res.*, *102*, 11,539–11,547, doi:10.1029/96JA03841.

Li, J., G. Ma, T. Maruyama, and Z. Li (2012), Mid-latitude ionospheric irregularities persisting into late morning during the magnetic storm on 19 March 2001, *J. Geophys. Res.*, *117*, A08304, doi:10.1029/2012JA017626.

Ma, G., and T. Maruyama (2006), A super bubble detected by dense GPS network at east Asian longitudes, *Geophys. Res. Lett.*, *33*, L21103, doi:10.1029/2006GL027512.

Makela, J. J., E. S. Miller, and E. R. Talaat (2010), Nighttime medium-scale traveling ionospheric disturbances at low geomagnetic latitudes, *Geophys. Res. Lett.*, *37*, L24104, doi:10.1029/2010GL045922.

Martinis, C., J. Baumgardner, J. Wroten, and M. Mendillo (2010), Seasonal dependence of MSTIDs obtained from 630.0 nm airglow imaging at Arecibo, *Geophys. Res. Lett.*, *37*, L11103, doi:10.1029/2010GL043569.

Martinis, C., J. Baumgardner, J. Wroten, and M. Mendillo (2011), All-sky imaging observations of conjugate medium-scale traveling ionospheric disturbances in the American sector, *J. Geophys. Res.*, *116*, A05326, doi:10.1029/2010JA016264.

Mendillo, M., J. Baumgardner, D. Nottingham, J. Aarons, B. Reinisch, J. Scali, and M. Kelley (1997), Investigations of thermospheric-ionospheric dynamics with 6300 Å images from the Arecibo Observatory, *J. Geophys. Res.*, *102*, 7331–7343, doi:10.1029/96JA02786.

Miller, C., W. Swartz, M. Kelley, M. Mendillo, D. Nottingham, J. Scali, and B. Reinisch (1997), Electrodynamics of midlatitude spread *F*: 1. Observations of unstable, gravity wave-induced ionospheric electric fields at tropical latitudes, *J. Geophys. Res.*, *102*, 11,521–11,532, doi:10.1029/96JA03839.

Miller, E. S., H. Kil, J. J. Makela, R. A. Heelis, E. R. Talaat, and A. Gross (2014), Topside signature of medium-scale traveling ionospheric disturbances, *Ann. Geophys.*, *32*, 959–965, doi:10.5194/angeo-32-959-2014.

Otsuka, Y., K. Shiokawa, T. Ogawa, and P. Wilkinson (2004), Geomagnetic conjugate observations of medium-scale traveling ionospheric disturbances at midlatitude using all-sky airglow imagers, *Geophys. Res. Lett.*, *31*, L15803, doi:10.1029/2004GL020262.

Park, J., K. W. Min, J.-J. Lee, H. Kil, V. P. Kim, H.-J. Kim, E. Lee, and D. Y. Lee (2003), Plasma blob events observed by KOMPSAT-1 and DMSP F15 in the low latitude nighttime upper ionosphere, *Geophys. Res. Lett.*, *30*(21), 2114, doi:10.1029/2003GL018249.

Park, J., C. Stolle, H. Lühr, M. Rother, S.-Y. Su, K. W. Min, and J.-J. Lee (2008), Magnetic signatures and conjugate features of low-latitude plasma blobs as observed by the CHAMP satellite, *J. Geophys. Res.*, *113*, A09313, doi:10.1029/2008JA013211.

Perkins, F. (1973), Spread *F* and ionospheric currents, *J. Geophys. Res.*, *78*, 218–226, doi:10.1029/JA078i001p00218.

Saito, A., T. Iyemori, M. Sugiura, N. C. Maynard, T. L. Aggson, L. H. Brace, M. Takeda, and M. Yamamoto (1995), Conjugate occurrence of the electric field fluctuations in the nighttime midlatitude ionosphere, *J. Geophys. Res.*, *100*, 21,439–21,451, doi:10.1029/95JA01505.

Saito, A., M. Nishimura, M. Yamamoto, M. Yamamoto, S. Fukao, T. Tsugawa, Y. Otsuka, S. Miyasaki, and M. C. Kelley (2002), Observations of traveling ionospheric disturbances and 3-m scale irregularities in the nighttime *F*-region ionosphere with the MU radar and a GPS network, *Earth Planet Space*, *54*, 31–44.

Seemala, G. K., and C. E. Valladares (2011), Statistics of total electron content depletions observed over the South American continent for the year 2008, *Radio Sci.*, *46*, RS5019, doi:10.1029/2011RS004722.

Shiokawa, K., Y. Otsuka, C. Ihara, T. Ogawa, and F. J. Rich, (2003), Ground and satellite observations of nighttime medium-scale traveling ionospheric disturbance at midlatitude, *J. Geophys. Res.*, *108*(A4), 1145, doi:10.1029/2002JA009639.

Shiokawa, K., et al. (2005), Geomagnetic conjugate observation of night-time medium-scale and large-scale traveling ionospheric disturbances: FRONT3 campaign, *J. Geophys. Res.*, *110*, A05303, doi:10.1029/2004JA010845.

Tsugawa, T., Y. Otsuka, A. J. Coster, and A. Saito (2007), Medium-scale traveling ionospheric disturbances detected with dense and wide TEC maps over North America, *Geophys. Res. Lett.*, *34*, L22101, doi:10.1029/2007GL031663.

Tsunoda, R. T., and R. B. Cosgrove (2001), Coupled electrodynamics in the nighttime midlatitude ionosphere, *Geophys. Res. Lett.*, *28*, 4171–4174, doi:10.1029/2001GL013245.

Valladares, C. E., and J. L. Chau (2012), The Low-Latitude Ionosphere Sensor Network (LISN) initial results, *Radio Sci.*, *47*, RS0L17, doi:10.1029/2011RS004978.

Valladares, C. E., and M. A. Hei (2012), Measurement of the characteristics of TIDs using small and regional networks of GPS receivers during the campaign of 17–30 July of 2008, *Int. J. Geophys.*, *2012*, 548784, 14, doi:10.1155/2012/548784.

Yokoyama, T., and D. L. Hysell (2010), A new midlatitude ionosphere electrodynamics coupling model (MIECO): Latitudinal dependence and propagation of medium-scale traveling ionospheric disturbances, *Geophys. Res. Lett.*, *37*, L08105, doi:10.1029/2010GL042598.

Yokoyama, T., D. L. Hysell, Y. Otsuka, and M. Yamamoto (2009), Three-dimensional simulation of the coupled Perkins and E_s-layer instabilities in the nighttime midlatitude ionosphere, *J. Geophys. Res.*, *114*, A03308, doi:10.1029/2008JA013789.